New Phytologist Supporting Information

An optimized genetically encoded dual reporter for simultaneous ratio imaging of Ca^{2+}- and H^+ reveals new insights into ion signaling in plants

Kunkun Li, Juan Prada, Daniel S.C. Damineli, Anja Liese, Tina Romeis, Thomas Dandekar, José A. Feijó, Rainer Hedrich and Kai Robert Konrad

article acceptance date: 23 December 2020

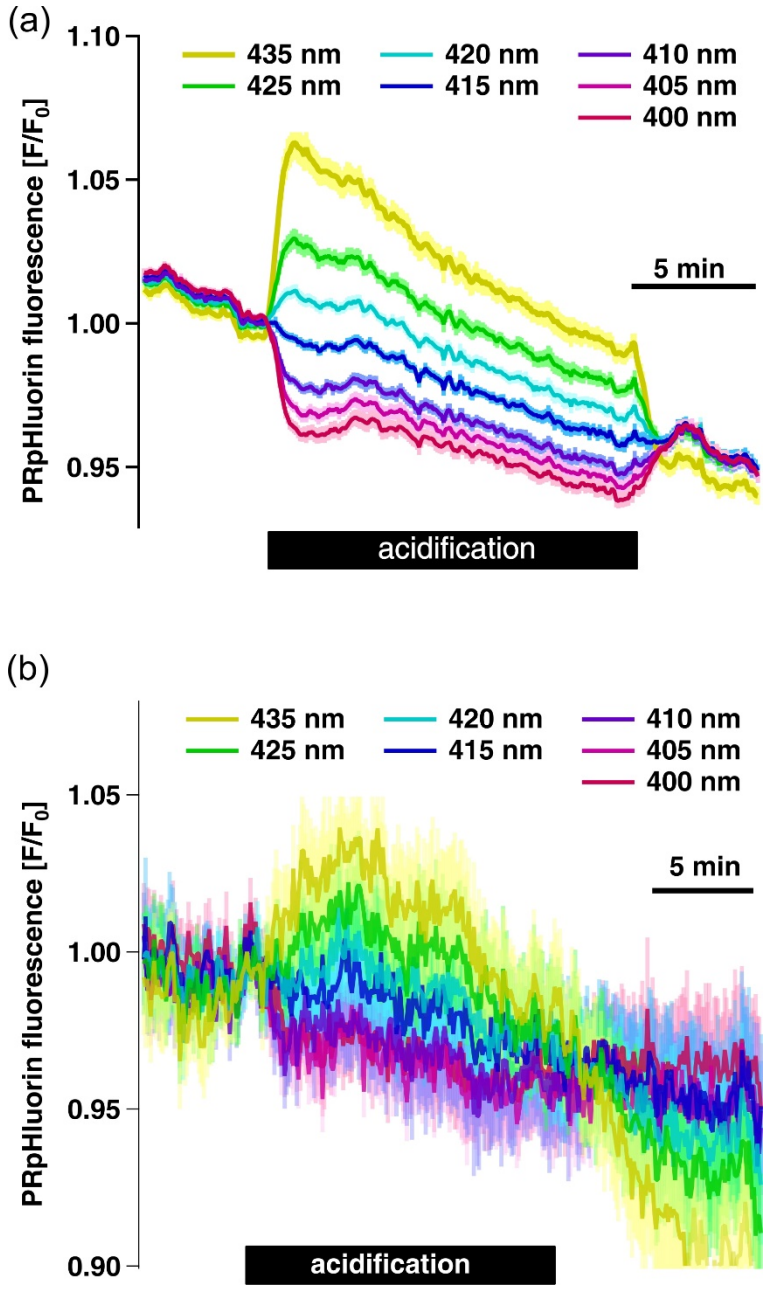

Figure S1. Isosbestic point of PRpHluorin in pollen tubes and guard cells

The PRpHluorin fluorescence over time is displayed upon cytosolic acidification in (a) GCs (n=50) and (b) PTs (n=16) when excitation light at each time-point was sequentially switched to wavelength as indicated by the colored traces. For PTs, the fluorescence was quantified from the apex with a modified version of the CHUKNORRIS algorithm. Acidification of the cytosol was achieved by transient application of 2 mM and 5 mM acetate in PTs and GCs, respectively, as indicated by the bar below the fluorescence traces. Error bars = SE.

(a)

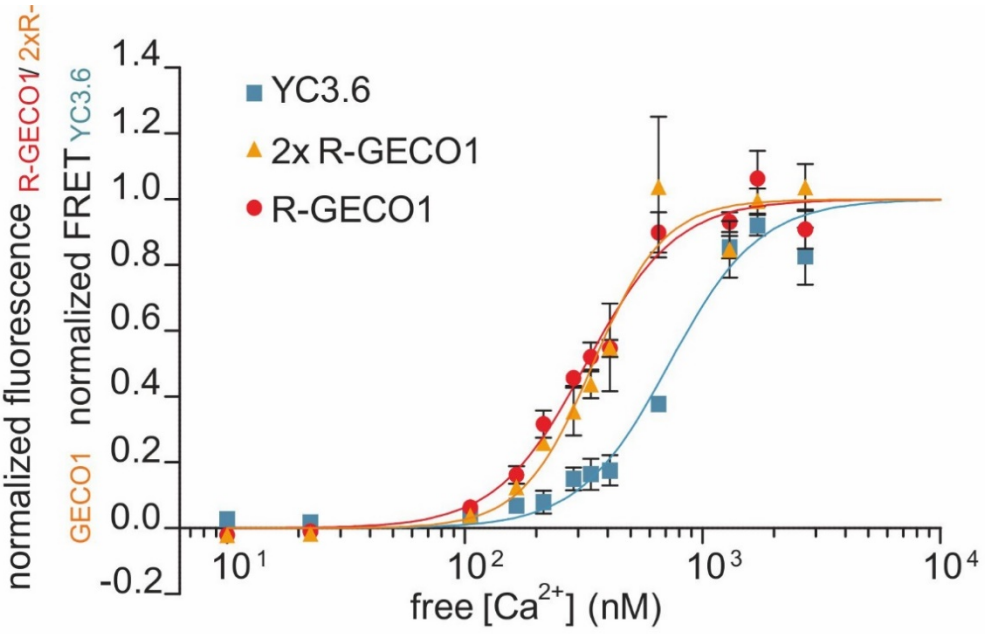

(b)

GECI variant	Ca^{2+} affinity EC50 (nM)		Hill coefficient		R^2
	Best-fit value	95% CI	Best-fit value	95% CI	
R-GECO1	329	308 to 352	2.36	1.94 to 2.78	0.91
2 x R-GECO1	352	313 to 396	2.66	1.76 to 3.55	0.76
YC3.6	719	671 to 770	2.12	1.89 to 2.35	0.92

Figure S2. Ca^{2+} binding to YC3.6 and R-GECO1 *in vitro*

(a) In vitro Ca^{2+} titration curves of R-GECO1, 2 x R-GECO1 and YC3.6. (mean ± SEM n=4-6, 12 Ca^{2+}-concentrations). One of two independent experiments is shown. For nonlinear regression fits of normalized fluorescence, bottom value was set to zero and top to one. EC_{50} values and Hill coefficients are fitted as shared values, among two independent experiments (global fit) with 3-6 technical replicates. Values are summarized in the table below (b). Graph pad prism computed 95 % confidence interval (CI).

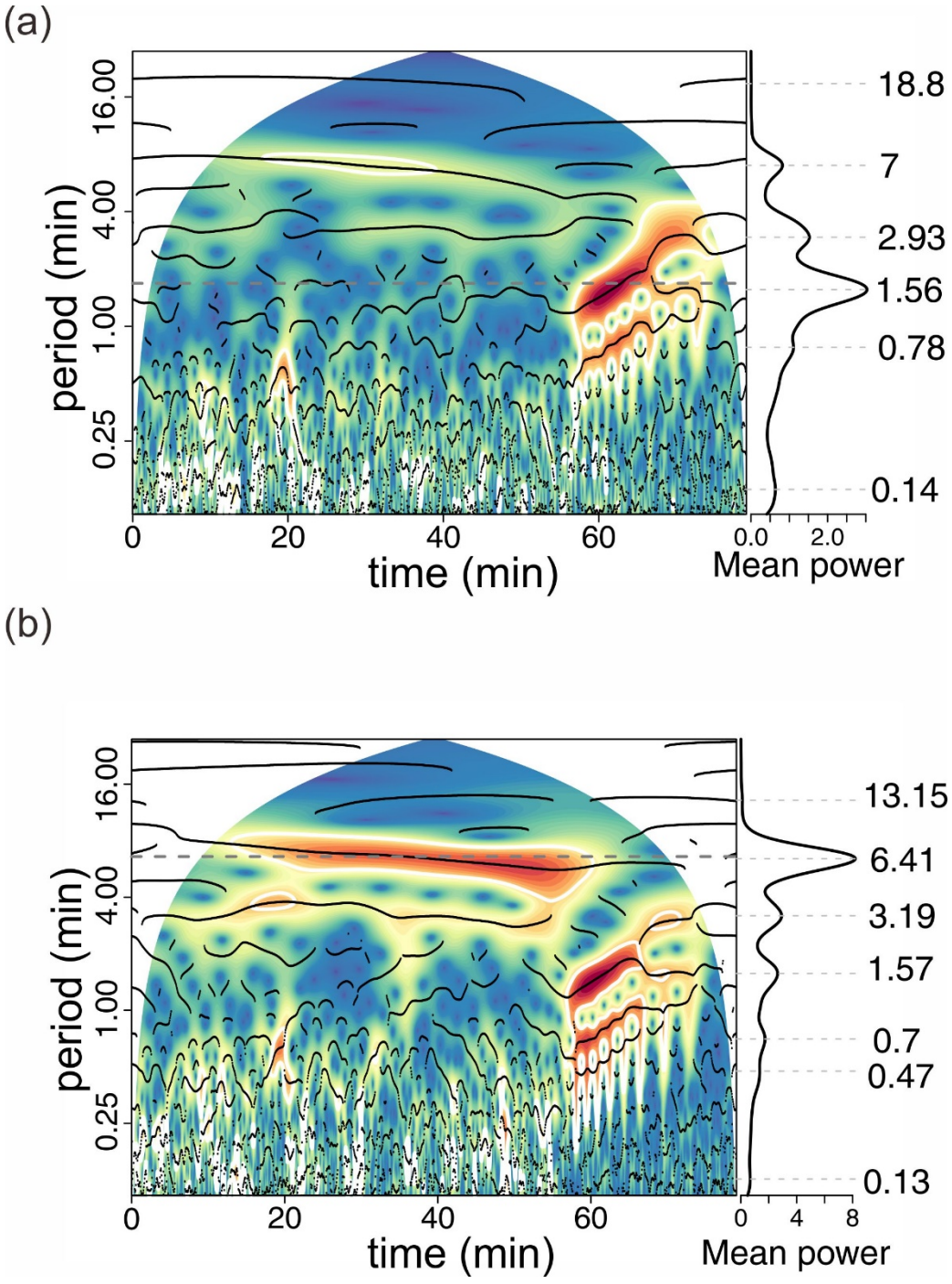

Figure S3. $[Ca^{2+}]_{cyt}$ and $[H^{+}]_{cyt}$ oscillations period in pollen tube under high Cl^{-} solution
(a and b) Continuous wavelet spectrum of the oscillation period dynamics (vertical axis, right side) and mean power of (a) the tip $[Ca^{2+}]_{cyt}$ and (b) $[H^{+}]_{cyt}$ of the same time-sequence over time received by wavelet transformation analysis of Fig.3a. The phase relationships reported are found on the ridges of the wavelet transformed and within the regions of statistical significance of the transformation as indicated by areas bordered by a white line in the wavelet spectra. Colors (from blue to red) correspond to the power of specific oscillatory components through time (time-frequency space) with significant ($p < 0.05$) areas bordered with a white line.

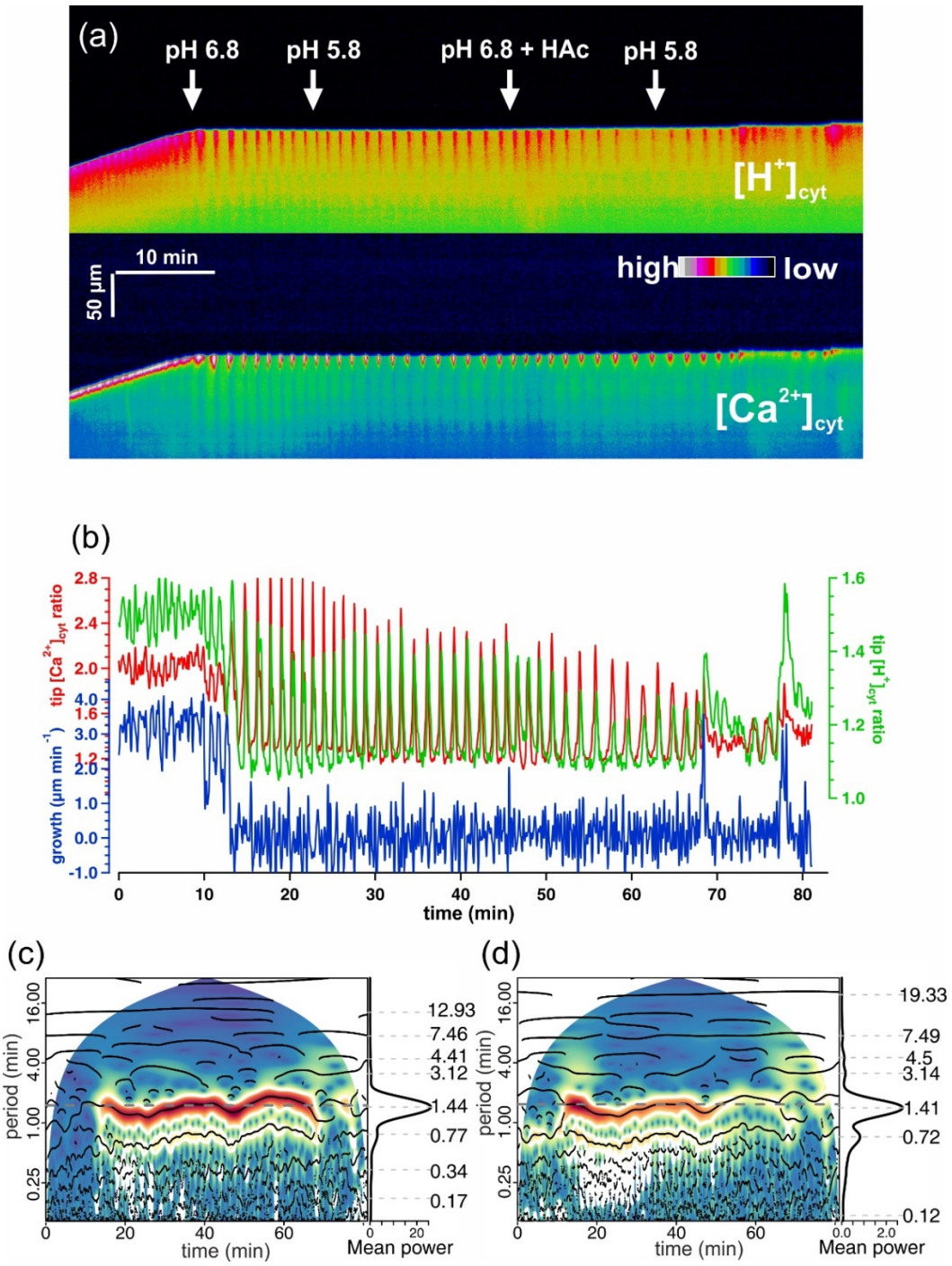

Figure S4. Pollen tube growth arrest is associated with tip $[Ca^{2+}]_{cyt}$ oscillations preceding $[H^+]_{cyt}$ oscillations, which is independent on the pH-gradient across the plasma membrane

CapHensor imaging of an example *N. tabacum* pollen tube challenged with different extracellular solutions to change the pH-gradient across the plasma membrane. (a) False colored kymographs showing the $[H^+]_{cyt}$ (top) and $[Ca^{2+}]_{cyt}$ (bottom) dynamics when the medium pH was changed as indicated or was supplemented with 2 mM Acetate (HAc) to acidify the cytoplasm. (b) Tip $[Ca^{2+}]_{cyt}$- (red) and $[H^+]_{cyt}$ (green) ratio signals and growth velocity (blue) plotted against the time from the cell shown in (a). Please note: during growth arrest, tip $[Ca^{2+}]_{cyt}$ oscillations precede tip $[H^+]_{cyt}$ oscillations with all media tested. (c and d) Wavelet spectra derived from wavelet transformations of (c) the tip $[Ca^{2+}]_{cyt}$- and (d) $[H^+]_{cyt}$ ratio signals from the experiment in (a) show stable $[Ca^{2+}]_{cyt}$ and $[H^+]_{cyt}$ oscillation periods (vertical axis, right). Colors (blue to red) correspond to the power of specific oscillatory components through time (time-frequency space) with significant ($p < 0.05$) areas bordered with a white line.

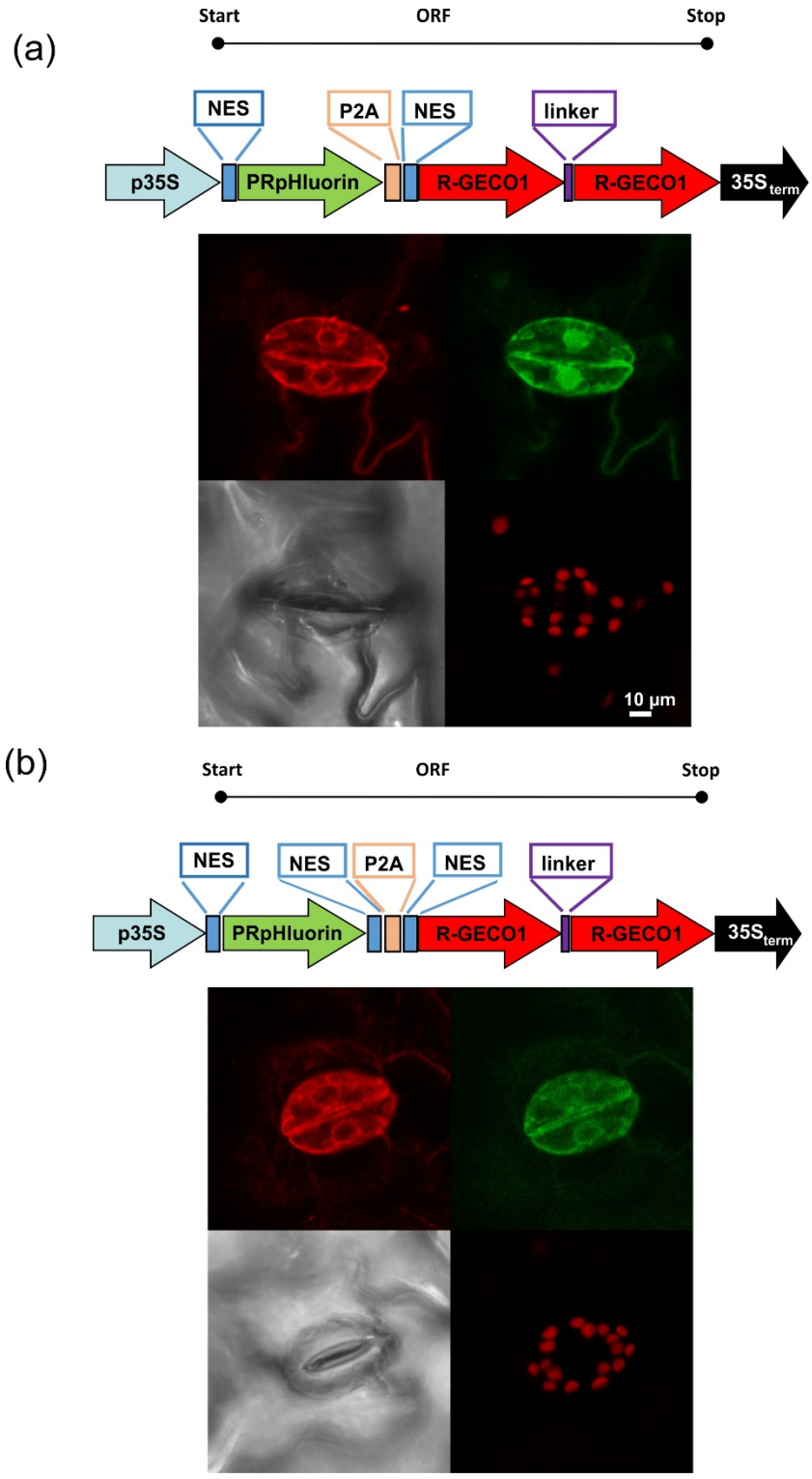

Figure S5. Subcellular localization of CapHensor versions in guard cells

Confocal images (Z-projections) of representative *Nicotiana tabacum* GCs expressing different multicistronic constructs harboring CapHensor versions. Upper part of figure (a) and (b) shows the vector design. The two vectors are basically the same, in (a) the N-terminus of PRpHluorin is equipped with a nuclear exclusion sequence (NES) while the vector in (b) harbors an additional NES-sequences at the C-terminus of PRpHluorin. Lower part of figure (a) and (b) shows R-GECO1- (red), PRpHluorin- (green), and chlorophyll (red) fluorescence as well as brightfield (gray) image. Note: green fluorescence of PRpHluorin shows cytosolic and nucleus localization in (a) while in (b) it resides in the cytosol only. Subcellular localization of red fluorescence demonstrates R-GECO1 to reside in the cytosol.

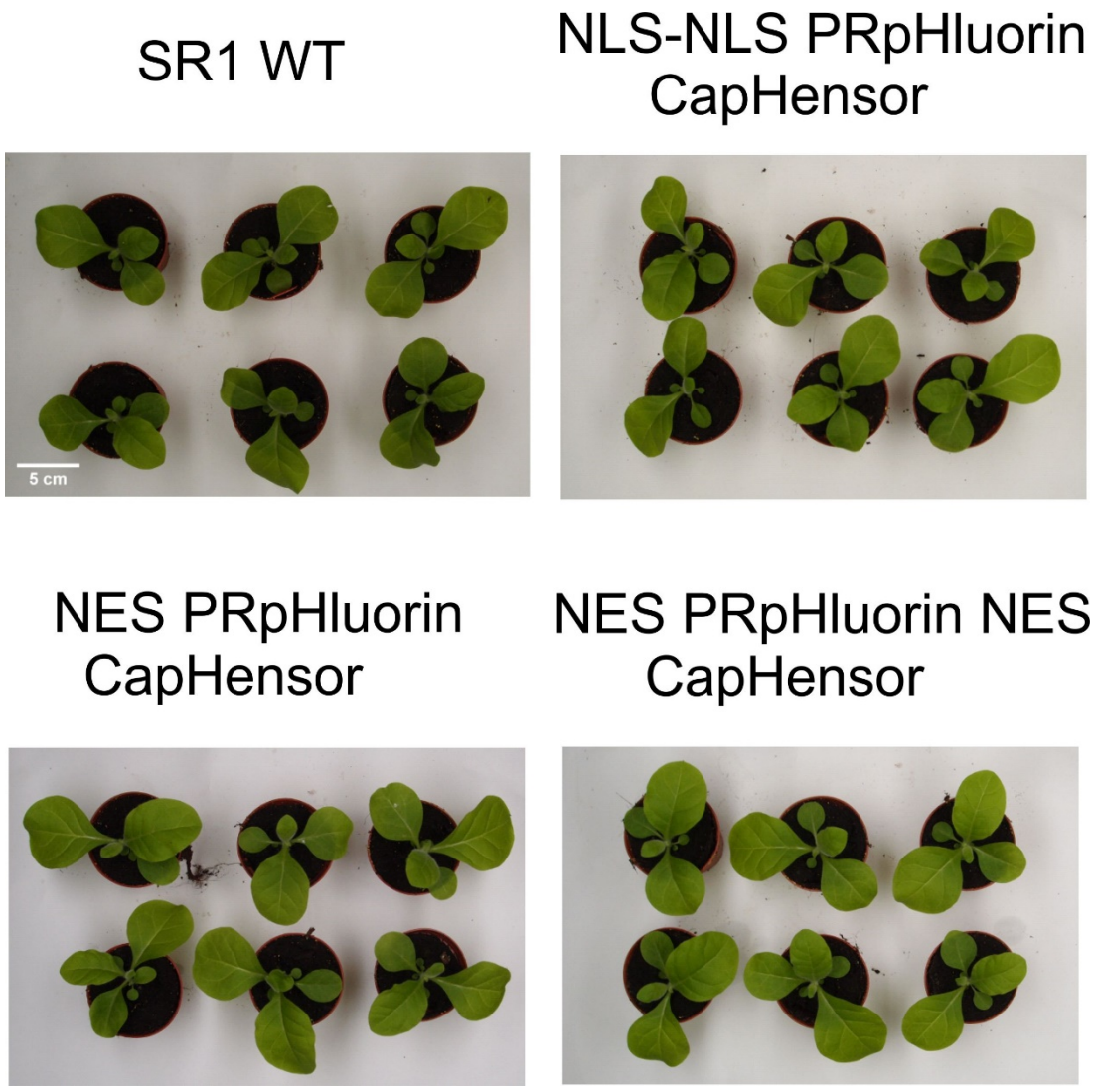

Figure S6. Transgenic *N. tabacum* CapHensor lines grow normal
Phenotype of 5-week-old *N. tabacum* plants grown side by side in the green house. WT plants and transgenic CapHensor expressing plants are compared. Six plants each are shown of wild type (SR1, variety Petite Havana) background (upper left), nucleus-targeted CapHensor (upper right, NLS-NLS CapHensor), cytosol-targeted CapHensor with N-terminal NES at the PRpHluorin (lower left) or N- and C-terminal NES at the PRpHluorin (lower right).

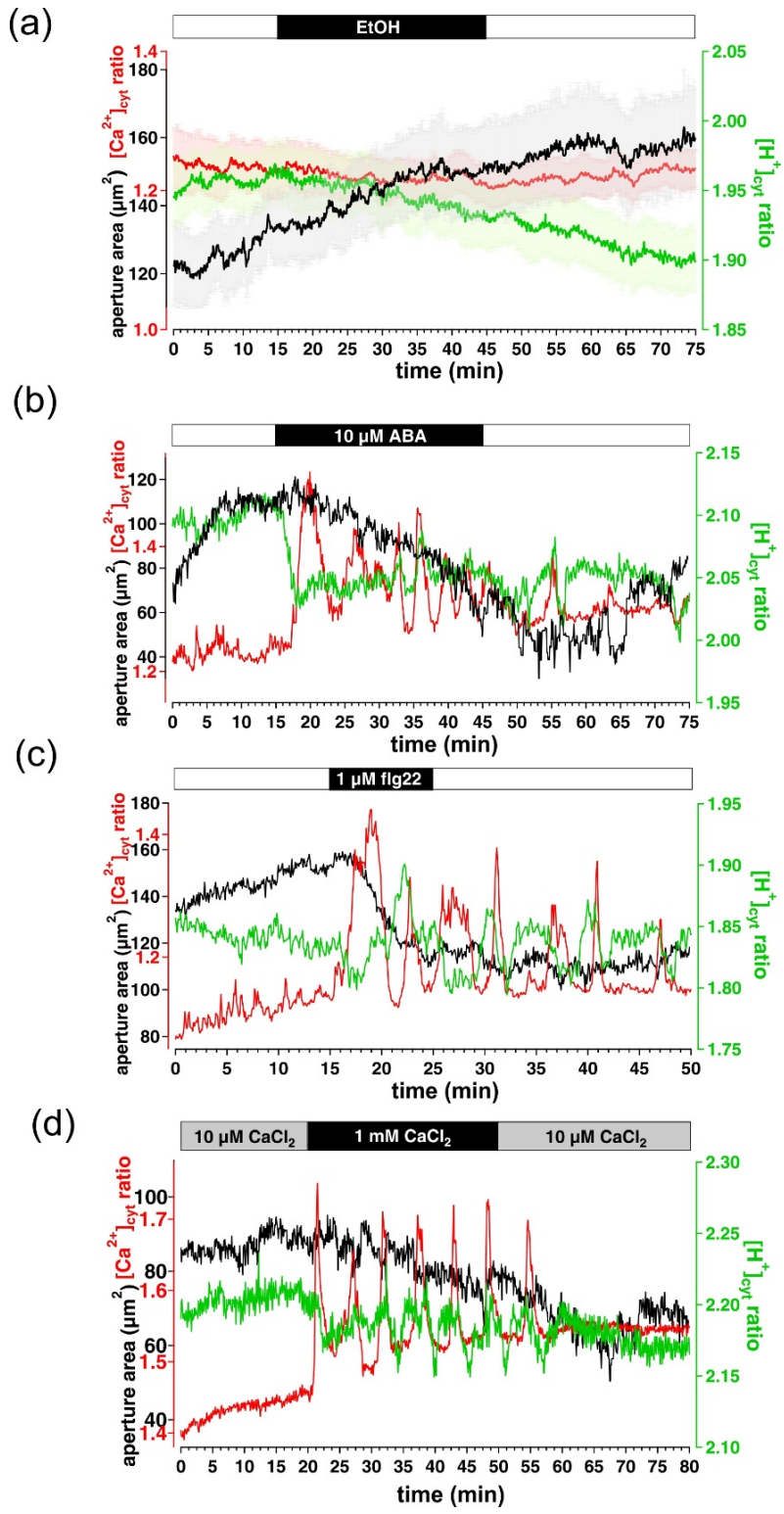

Figure S7. $[Ca^{2+}]_{cyt}$ and $[H^+]_{cyt}$ oscillations in individual guard cells upon ABA, flg22 and high Ca^{2+} treatment

Time-lapse CapHensor imaging together with stomata aperture monitoring in GCs of *N. tabacum* epidermal strips. (a) Mean $[Ca^{2+}]_{cyt}$ ratio (red), $[H^+]_{cyt}$ ratio (green) and stomatal aperture area (black) over time upon application of 0.005 % EtOH (n=16), which corresponds to the amount when treated with 10 µM ABA. (b-d) $[Ca^{2+}]_{cyt}$ ratio (red), $[H^+]_{cyt}$ ratio (green) and stomatal aperture area (black) over time in single representative guard cell upon application of (b) 10 µM ABA,(c) 1 µM flg22 and (d) increasing Ca^{2+}-concentration via perfusion from 10 µM $CaCl_2$ to 1 mM $CaCl_2$.

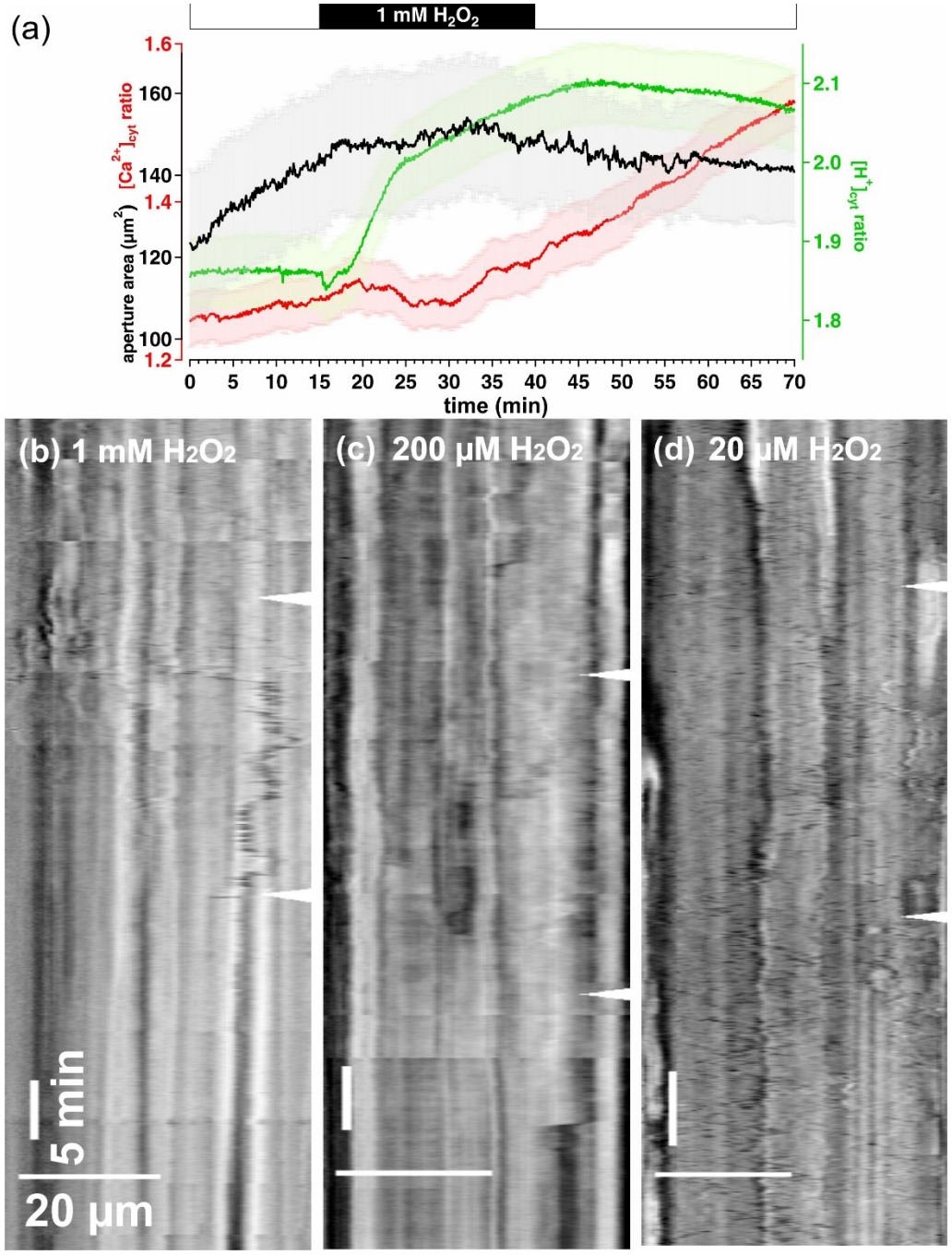

Figure S8. 1 mM H_2O_2 results in loss of guard cell integrity

Time-lapse CapHensor imaging together with stomata aperture monitoring in GCs of *N. tabacum* epidermal strips. (a) Mean $[Ca^{2+}]_{cyt}$ ratio (red), $[H^+]_{cyt}$ ratio (green) and stomatal aperture area (black) over time upon application of 1 mM H_2O_2 (n=18). Error bars = SE. (b-d) Brightfield kymographs of a representative guard cell treated with (b) 1 mM H_2O_2, (c) 200 µM H_2O_2 and (d) 20 µM H_2O_2. White marks on the right side of the kymographs indicate the time of H_2O_2 treatment and wash out. Note: Cytoplasmic streaming results in a noisy pattern within the kymograph, whereas slow-moving or aggregated cytoplasm after loss of cell vitality results in distinct and constant patterning of the kymograph.

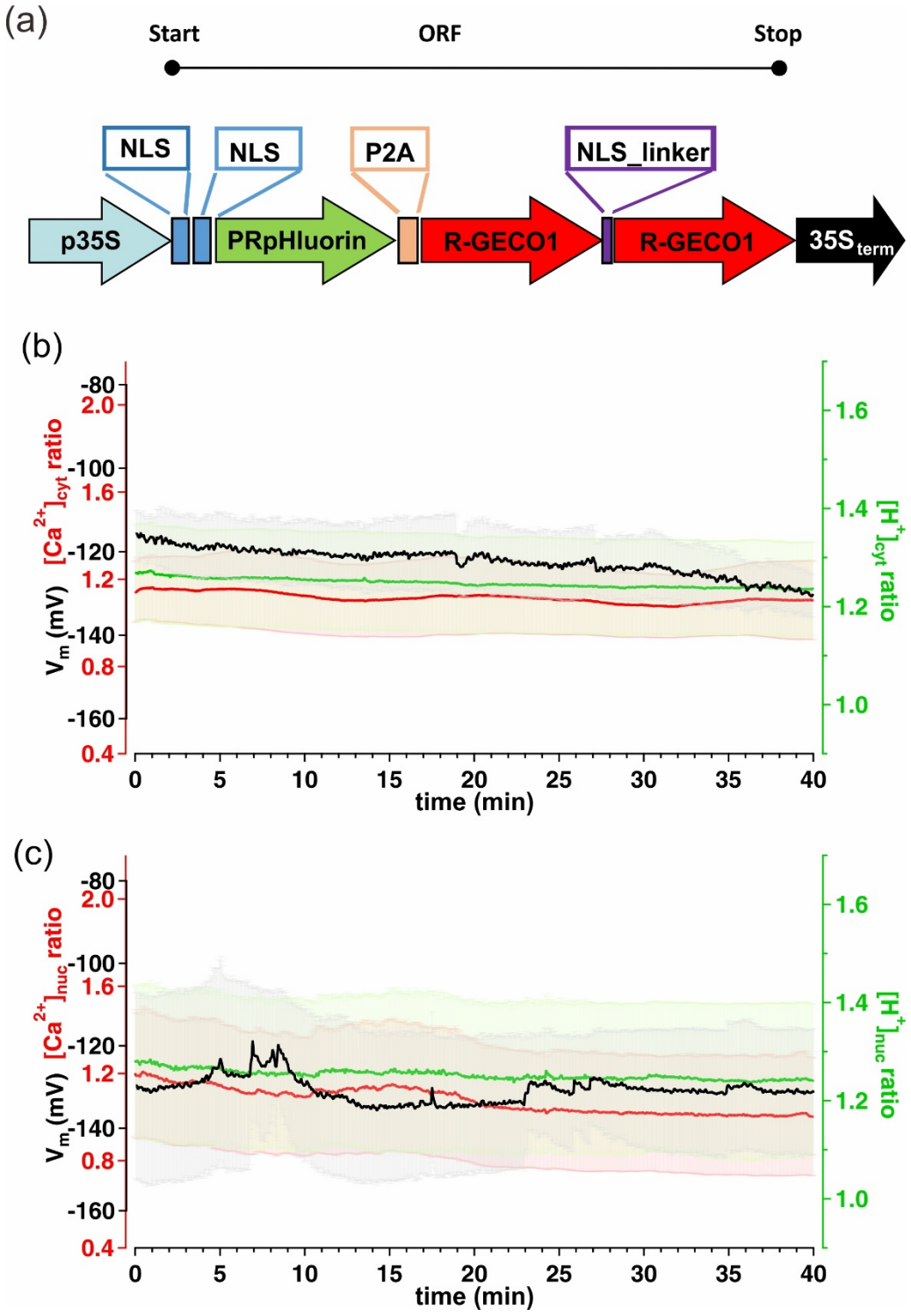

Figure S9. Ca^{2+}, H^+ and V_m regime in the mesophyll under control conditions
Simultaneous Ca^{2+}, H^+ and membrane voltage (V_m) recordings in mesophyll cells of *N. benthamiana* leaves transiently expressing a cytosolic- or nuclear version of the CapHensor. (a) The vector design to localize the CapHensor in nuclei. The N-terminus of PRpHluorin in the CapHensor construct is equipped with two different nuclear localization sequences (NLS). Additionally, a NLS is sandwiched by the two R-GECO1s. (b) Mean $[Ca^{2+}]_{cyt}$ ratio (red), $[H^+]_{cyt}$ ratio (green) and V_m (black) under control conditions (n=4). (c) Mean $[Ca^{2+}]_{nuc}$ ratio (red), $[H^+]_{nuc}$ ratio (green) and V_m (black) under control conditions (n=3). Error bars = SE.

Table S1. Primers used for cloning CapHensor versions

Cloning Primers	Sequences
CapHensor NLS	
NLSNLS PR User pHluorin fwd	GGCTTAAUATGCCAAAAAAGAAGAGAAAGGTAGAAGACCCCATGCCAAAGAAGAAGCGTAAGGTAAGT
Long NLS PR pHluorin User fwd	GGCTTAAUATGCCAAAAAAGAAGAGAAAGGTAGAAGACCCCAGTAAAGGAGAAGAACTTTTCACTGGAG T
P2A pHluorin User rev	AGCCTGCTUCAGCAGGCTGAAGTTAGTAGCTCCGCTTCCTTTGTATAGTTCATCCATGCCATG
P2A half R-GECO1 fwd	AAGCAGGCUGGAGACGTGGAGGAGAACCCTGGACCTATGGTCGACTCTTCACGTCGTAAG
NLS-linker R-GECO1 rev	ACCTTTCTCUTCTTTTTTGGAGGCTTCGCTGTCATCATTTGTACAAACT
NLS-linker R-GECO1 fwd	AGAGAAAGGUAGAAGACCCCGGGGATCCACCGGTCGCCACCGTCGACTCTTCACGTCGTAAGTGG
RGECO1 User rev	GGTTTAAUCTACTTCGCTGTCATCATTTGTACAAA
CapHensor NES	
pHluorin half NES User rev	AGCTTCTTCUGCAAGGCCACCGCTTTGTATAGTTCATCCATGCCATGT
NES USER fwd	GGCTTAAUATGCTGCAGAACGAGCTTGC
P2A half NES User fwd	AGAAGAAGCUGGAGGAGCTAGAGCTTGGAAGCGGAGCTACTAACTTCAGC
RGECO1 RGECO1 User rev	ACTGAGGTTUAATCCCTTCGCTGTCATCATTTGTACAAAC
RGECO1 RGECO1 User fwd	AAACCTCAGUGGTGGAATGGTCGACTCTTCACGTCGT
RGECO1 User rev	GGTTTAAUCTACTTCGCTGTCATCATTTGTACAAA
Half NES pHluorin fwd	ACAAGACUGGAGGAGTCGACTCGAGTGCGGCCGCCACCATGAGTAAAGGAGAAGAACTTTTCACTG
LeLAT half NES rev	AGTCTTGUTAATATCAAGTCCAGCCAACTTAAGAGCAAGCTCGTTCTGCAGCATTTTTTTTTTGGTGTGTGTACTTTTTTTT
UBQ10 half NES rev	AGTCTTGUTAATATCAAGTCCAGCCAACTTAAGAGCAAGCTCGTTCTGCAGCATGATCCCGCACTCGAGCTGT
P2A half NES rev	AGTCTTGUTAATATCAAGTCCAGCCAACTTAAGAGCAAGCTCGTTCTGCAGCATAGGTCCAGGGTTCTCCTCCAC
Half NES R-GECO1 fwd	ACAAGACUGGAGGAGTCGACTCGAGTGCGGCCGCCACCATGGTCGACTCTTCACGTCGTAA
Sequencing primers	
UBQ10 seq fwd	TGTCGAATAATTACTCTTCG
pHluorin CT seq fwd	CGAAAGATCCCAACGAAAAG
R-GECO1 NLS-linker seq fwd	TGACAGCGAAGCCTCCAAAAA
R-GECO1 NLS-linker seq rev	GAGTCGACGGTGGCGACC
pHluorin User rev	GGTTTAAUTTATTTGTATAGTTCATCCATGCCATG
35S Terminator rev	GGT TTA AUG TCA CTG GAT TTT GGT TTT AGG AAT TAG

RGECO1 RGECO1 seq rev	TTCCACCACTGAGGTTTAATCCC
RGECO1 RGECO1 seq fwd	GGGATTAAACCTCAGTGGTGGAA
LeLAT52 seq fwd	CAAGACACACACAAAGAGAAGGAG
R-GECO1 mid seq rev	CCC TCG ATC TCG AAC TCG TG
RBC seq rev	GTG CGC AAT GAA ACT GAT GC

Video S1.

Time-lapse CapHensor imaging of a representative *N. tabacum* PT from Fig. 2a, b with false colored $[H^+]_{cyt}$- (top) and $[Ca^{2+}]_{cyt}$ (bottom) ratio, and widefield image (bottom) upon sequential extracellular medium perfusions of different pH or low osmolarity (hypo shock).

Video S2.

Time-lapse CapHensor imaging of a representative *N. tabacum* PT from Fig. 2d, e with false colored $[H^+]_{cyt}$- (top) and $[Ca^{2+}]_{cyt}$ (bottom) ratio, and widefield image (bottom) upon 3 mM caffeine perfusion.

Video S3.

Time-lapse CapHensor imaging of a representative *N. tabacum* PT from data presented in Fig. 3a, b with false colored $[H^+]_{cyt}$- (top) and $[Ca^{2+}]_{cyt}$ (bottom) ratio, and widefield image (bottom). Extracellular medium Cl^--increase from 10 mM Cl^- to 20 mM Cl^- (t=10 min) and later (t=55 min) alkalization of the medium (pH 6.8) was performed.

Video S4.

Time-lapse CapHensor imaging of a representative *N. tabacum* GC in epidermal strip. Movie corresponds to data presented in Fig. 4a with false colored $[H^+]_{cyt}$- (top) and $[Ca^{2+}]_{cyt}$ (middle) ratio, and widefield image (bottom). Extracellular application of 10 µM ABA at t=15-45 min was performed. Please note the decrease in $[H^+]_{cyt}$-ratio, increase in $[Ca^{2+}]_{cyt}$-ratio together with stomatal closure during the presence of 10 µM ABA. Upon wash-out of ABA the stoma re-opens.

Video S5.

Time-lapse CapHensor imaging of a representative *N. tabacum* GC in epidermal strip. Movie corresponds to data presented in Fig. 4d with false colored $[H^+]_{cyt}$- (top) and $[Ca^{2+}]_{cyt}$ (middle) ratio, and widefield image (bottom). Extracellular application of 1 µM flg22 at t=15-25 min was performed. Please note the unaltered $[H^+]_{cyt}$-ratio, but strong

increase in $[Ca^{2+}]_{cyt}$-ratio together with stomatal closure upon 1 µM flg22 treatment. Upon wash-out of 1 µM flg22 the stoma does not re-open.

Video S6.

Two time-lapse CapHensor imaging series of representative *N. tabacum* GCs in epidermal strips upon 200 µM H_2O_2 (left side) or 1 mM H_2O_2 (right side) treatment, arranged next to one another. Movies correspond to data presented in Fig. 4g and Fig. S8 and show false colored $[H^+]_{cyt}$- (top) and $[Ca^{2+}]_{cyt}$ (middle) ratio, as well as widefield images (bottom). The time course of H_2O_2 application (t=15-40 min) is the same for both cells. Please note the strong increase in $[H^+]_{cyt}$-ratio but unaltered $[Ca^{2+}]_{cyt}$-ratio and stomatal aperture with 200 µM H_2O_2, but increase in $[H^+]_{cyt}$- and $[Ca^{2+}]_{cyt}$-ratio together with stomatal closure upon 1 mM H_2O_2 application. Important to note is that steep $[H^+]_{cyt}/[Ca^{2+}]_{cyt}$-ratio increase and stomatal closure is caused by loss of cell integrity upon 1 mM H_2O_2 application, visible by the lack of cytoplasmic streaming within the brightfield (see also Fig. S8) and ratio images.

Video S7.

Two time-lapse imaging series of representative *N. benthamiana* mesophyll tissue when expressing the cytosolic or nuclear version of the CapHensor are arranged next to one another. The response to 0.1 µM flg22 with the same time course is presented and correspond to data presented in Fig. 6 b and f. False colored $[H^+]$- (top) and $[Ca^{2+}]$ (middle) ratio images as well as the brightfield images (bottom) of mesophyll tissue expressing the cytosolic- (left row) or nuclear (right row) CapHensor version. Please note the strong increase in $[H^+]_{cyt}$- and $[Ca^{2+}]_{cyt}$-ratio in areas of the cytosol or nuclei after flg22-treatment when expressing the cytosolic or nuclear version of the CapHensor, respectively.

Notes S1. R-scripts for quantitative analysis of data from pollen tubes, guard cells and mesophyll cells. A zip-file is provided as supporting information, including three folders with R-scripts and example files for analysis as well as a Microsoft Word document with explanations on how to use those R-scripts.